BioChip Journal (2022) 16:305–316
https://doi.org/10.1007/s13206-022-00068-x

ORIGINAL ARTICLE

Biological Influence of Pulmonary Disease Conditions Induced by Particulate Matter on Microfluidic Lung Chips

Faiza Jabbar[1] · Young-Su Kim[2] · Sang Ho Lee[3]

Received: 15 December 2021 / Revised: 4 May 2022 / Accepted: 15 June 2022 / Published online: 8 July 2022

Abstract

Particulate matter (PM10)-induced respiratory illnesses are difficult to investigate in trans-well culture systems. Microphysiological systems offer the capacity to mimic these phenomena to analyze any possible hazards that PM10 exposure poses to respiratory system of Humans. This study proposes an on-chip healthy human lung distal airway model that efficiently reconstitutes in vivo-like environmental conditions in a microfluidic device. The lung-on-chip model comprises a TEER sensor chip and portable microscope for continuous monitoring. To determine the efficacy of our model, we assessed the response to exposure to three PM environmental conditions (mild, average, and severe) and analyzed the relevant in vivo physiological and toxicological data using the airway model. Our results revealed significant increases in the levels of the IL-13, IL-6, and MUC5AC pathological biomarkers, which indicate increased incidences of on-chip asthma and chronic obstructive pulmonary disease conditions. Overall, we deduced that this model will facilitate the identification of potential therapeutics and the prevention of chronic life-threatening toxicities and pandemics such as COVID-19. The proposed system provides basic data for producing an improved in organ-on-chip technology.

Keywords Microfluidic · Distal airways · TEER · Real-time monitoring · IL-13 · IL-6 · Particulate matter

1 Introduction

Particulate matter (PM10) has become a chief distress due to its elevated levels in air, which correlate with the greater number of breathing illnesses in cosmopolitan cities. Epidemiological and toxicological studies indicate that particulate matter is a primary cause of lethal respiratory diseases and mortality at an early age [1]. Stress catalysts (PM10, smoke, Dust and chlorofluorocarbons CFC's) in environment are convoluted in developing airway illnesses, i.e., chronic obstructive pulmonary disease (COPD), asthma and interstitial lung diseases [2]. PM10 aggravates respiratory illnesses and affects bronchiolar and alveolar passages health. PM10 resides in the human airways, and its deposition leads to serious respiratory illnesses, whereas PM2.5 is responsible for harming the circulatory system as it can cross the alveolar capillary barrier. Moreover, mounting evidence suggests that tumor necrosis factor-alpha (TNF-α) and interleukin-6 (IL-6) are key factors causing inflammation of airways [3–5].

Exposure of allergens causes asthma which is linked with TH-2 inflammation along with IL-13. Key cytokines are the most important factors for inflammation and remodeling of this immune response [6]. Due to the lack of pathophysiological relevance, animal models for respiratory diseases are being replaced with high-throughput microfluidic microphysiological systems (MPSs) [7]. The organ-on-chip technology is supportive for discovery of physiologically relevant organs. MPSs recapitulate human physiology at cellular level and access diseased and stressed conditions in biochemically and mechanically controlled dynamic fluid flow conditions [8].

The development of organ chips with the integration of real-time sensors has the potential to simultaneously mimic and monitor cell health [9, 10]. One of the cellular development monitoring techniques is trans-epithelial

Faiza Jabbar and Young-Su Kim have contributed to this work equally.

✉ Sang Ho Lee
leesangho@jejunu.ac.kr

[1] Advanced Micro Mechatronics Lab, School of Engineering, Jeju National University, Jeju, Republic of Korea

[2] BioSpero, Inc., Jeju, Republic of Korea

[3] College of Pharmacy, Jeju National University, Jeju, Republic of Korea

electrical resistance (TEER), which determines cell proliferation by electrical impedance across the epithelium [11]. Recently, the TEER system was used to analyze and measure integrity of monolayers of cells. For trans-well culture systems, this is a basic measurement technique; however, its integration into transparent microfluidic chips remains a challenge for the medical field. By techniques of conventional metal patterning cell culture chambers are erected on organ-on-chip microfluidic culture devices around electrodes and the integration of glass and polymeric substances [12–14]. The TEER electrode location effects the changes in TEER values in cultures [14–16]. Microfluidic chip design and simulations are also playing important role in symmetry of the cell and velocity of the fluids in microfluidic systems [17]. Microfluidic systems with embedded sensors are increasingly being developed owing to their rapid efficacy testing capacity; for example, strain sensors and humidity sensors for health tracking and production of implantable applications [18].

This study introduces a microphysiological system with a human lung distal airways-on-a-chip model, an ITO-printed glass chip for TEER sensor along with inhouse built monitoring microscope for continuous monitoring for imaging as shown in Fig. 1a. To create daily human exposure conditions to PM10, three different particulate matter concentrations (mild, average, and severe) were allowed to pass through the organ-on-chip after stable culture of distal airway cells on a chip as described in Fig. 1b. Inflammatory response in human small airway cells triggered by PM10 exposure represented impedance variations correlating with analysis of confocal microscope of cytokine secretion, and reactive oxygen species (ROS) levels also showed degradation monolayer and its permeability by dose-dependent oxidative damage.

To test the exposure of particular matter, the platform was configured as shown in Fig. 1a, and the original image was displayed. The platform consisted of a peristaltic pump, media reservoir, bubble trap, CO_2/temperature control module, microscope, and chip. After four days of stable culture of (SAEC's, HPAEpiC's) on the normal chip was observed, for the monolayer permeability. This evaluation by impedance values was performed by the TEER sensor along with the real-time microscope. Twelve chips representing mild (7.50 µg/ml), average (37.55 µg/ml), and severe (151.5 µg/ml) conditions of PM10 were exposed to the culture medium containing PM10 for a 8 h for 4 d of the working days to recapitulate the circadian exposure of the human lung to PM, and media was then traded with the medium not exposed to PM10. All chips were exposed to identical culturing conditions (except for different PM concentrations), excluding the control chip (Fig. 1b).

2 Results and Discussion

2.1 PM Characterization

The PM10 analyzed in this study predominately comprised PAHs, dioxins, PCBs, zinc, cadmium, mercury, cobalt, and SiO_2. Moreover, SEM analysis confirmed that the particle size of the PM10 was < 10 µm, as shown in Fig. 2.

2.2 Barrier Integrity Demonstrated by Impedance Data

The impedance data of TEER sensor revealed a positive increase in values of barrier junctions along with confluency of cells after half hour on positive control chips. Impendence data further revealed escalation in confluency of epithelial

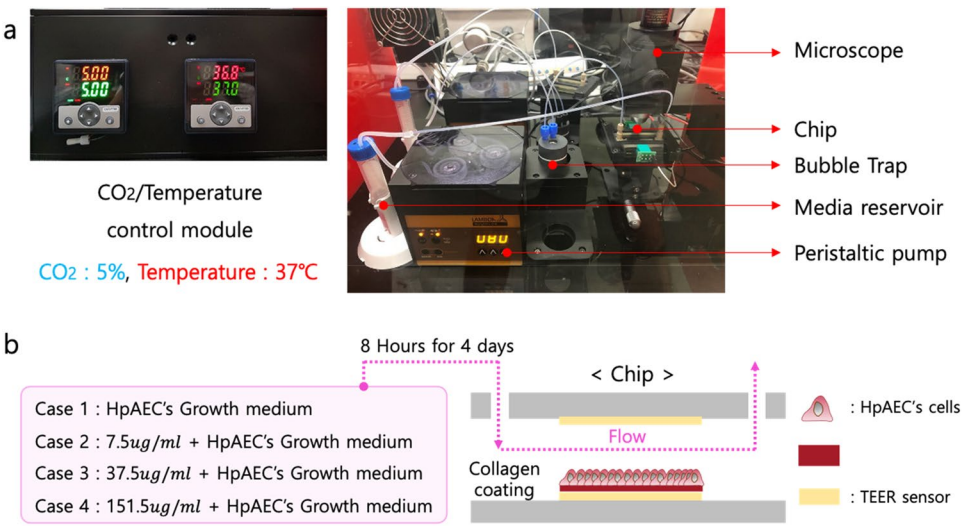

Fig. 1 **a** Organ-on-chip platform attached with peristaltic pump and portable microscope, with controlled temperature and carbon dioxide; **b** particulate matter exposure scheme representing four different cases. The first case represents positive control with normal growth medium, case 2 represents the mild condition with PM10 concentration of 7.5 µg/ml, case 3 indicates an average condition with a relatively high PM10 concentration (37.5 µg/ml), and a severe condition is indicated in case 4 with high PM10 concentration of 151 µg/ml

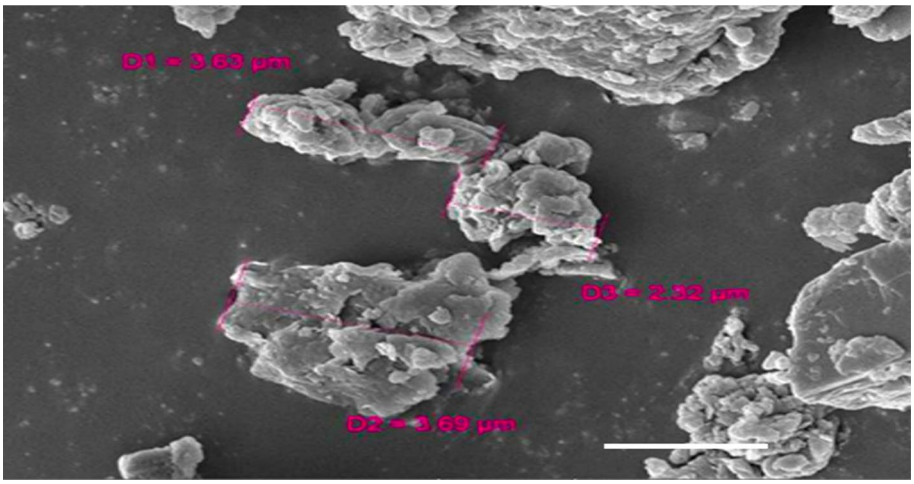

Fig. 2 Scanning electron micrograph of PM10 components, namely ERM-CZ-100 organic, ERM-CZ-120 inorganic, respectively, used in this study. Scale bar: 2 µm

cell junctions. Confluency of stable cultures enhanced after 4 days. The impedance value of the confluent monolayer was 930 Ω cm^2, consistent with average impedance values reported in a previous study (800–980 Ω cm^2) [8]. Specific values could be obtained from the lung-on-chip experiment conducted in this study as the ITO-printed chip for TEER sensor facing straight the surface of the cells, several reports have demonstrated TEER impedance readings in trans-well cell culture systems, and the system integrated sensor approach was first introduced in our MPS, as shown in Fig. 3a.

2.3 Monolayer Membrane Integrity Epithelium Barrier Properties

Confocal microscopy was used for immunofluorescence analysis which revealed excellent growth environment provided by the platform. As a result, a complete monolayer of lung epithelial cells was constructed. Mucus-producing, ciliated pseudostratified epithelium cells were observed in the layer. Their predomination indicated fresh production and were characterized by epithelial cell markers with the help of MUC5AC for goblet cells and anti-β tubulin IV for ciliated cells, as shown in Fig. 3c. The evaluation of integrity and epithelial tight junction of the lung epithelial monolayer was achieved by stained cells on a glass chip with occludin antibody-conjugated Alexa Fluor 594 (Sigma), as shown in Fig. 3b. Confocal micrograph results indicate complete monolayer integrity along with no damage to morphology of lung epithelium in microfluidic platform. The results complemented TEER sensor impedance values.

2.4 Damage to Barrier Integrity after PM Exposure

High concentration of PM disrupts barrier functions, as indicated by the confocal micrographs in Fig. 4, while low PM concentrations (7.5 µg/ml) result in expression of epithelial cell junction markers on the control chip (Fig. 4a). Barrier permeability loss was recorded at high concentrations (37.5 µg/ml and 151 µg/ml), as seen in Fig. 4b–d, previously indicated by TEER and cytokine analysis measurements. Real-time microscopy images showing low cell viability in PM-treated chips compared to the control chips are shown in Fig. 2 (Supplementary Data).

2.5 Confocal Microscopy of Ciliated Cells Dysfunction and Hyperplasia Goblet Cell

Respiratory disease patient secretes a protein molecule MUC5AC, which is a polymeric mucin MUC2 of a low charge glycoform. Moreover, inflammation leads to mucin hypersecretion which clogs airways causing COP and cystic fibrosis (CF) [19, 20]. Disruption of airway hemostasis in ciliated cells causes Goblet cell hyperplasia by shutting down clearance of mucociliary passage along with macrophage activation. This ultimately results in chronic pulmonary diseases (Fig. 5b–d). The high expression mucin (MUC5AC) was attributed to PM concentrations. The PM-treated along with untreated (control) chip revealed increase in mucin production dependent on dose. This further strengthened the fact that exposure to PM causes asthma, COPD, along with hyper-responsiveness of the airway, while alternatively PM also limits the expression of anti-β tubulin IV, decreased ciliary beating frequency and clearance of mucociliary (Fig. 5h). One of the most integral function of homeostasis in distal airway epithelial ciliated and goblet cells (Fig. 3b, c).

2.6 Reactive Oxygen Species Estimation

PM exposure causes damage to lung cells [21]. The most common airborne components in PM10 are Co, Ni, Cr, Mn, Zn, Cu, and Fe [22]. Iron (Fe) causes oxidative stress and assists the alteration of (O_2^-) superoxide anions and (H_2O_2)

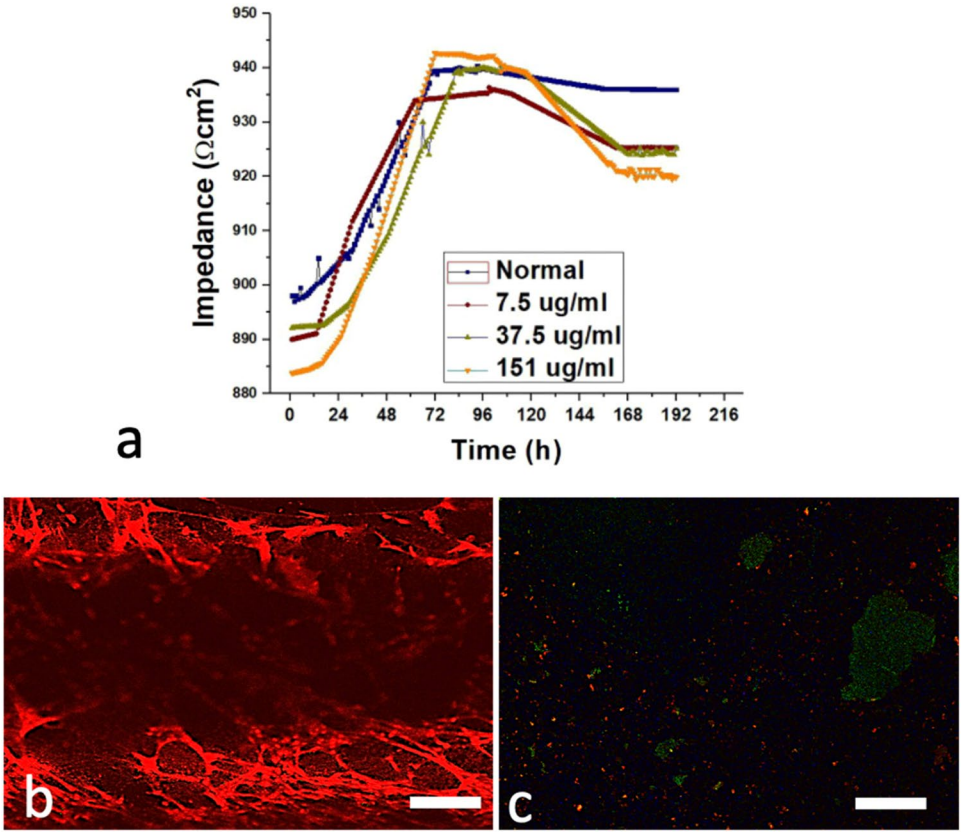

Fig. 3 **a** Impedance values of healthy lung epithelial junctions vs. experimental time. The blue line indicates the impedance values of the normal chip and shows a complete experimental impedance pattern of the stability of tight junctions achieved on day 3. The red line shows the impedance values vs. time for a PM10 concentration of 7.5 µg/ml, indicating a slight drop in the impedance values. The green line represents the impedance values for a relatively high PM10 concentration (37.5 µg/ml). The orange line shows a significant decline in the impedance values at a high PM10 concentration of 151 µg/ml. **b**, **c** Alveolar epithelium, AT type-I goblet cells stained with MUC5AC (Green) and AT type-II ciliated cells stained with Antiβ tubulin IV (Red; scale bar: 100 µm; **a** epithelial tight junctions stained with occludin conjugated Alexa Fluor 594; and **b** lung on chip showing epithelium, small lung airway, and alveolar epithelial goblet cells stained with MUC5AC (Green) and ciliated cells stained with anti-β tubulin IV (Red). Scale bar: 100 µm

hydrogen peroxide to (OH^-) hydroxyl ions [23]. PM10 exposure leads to surfactant dysfunction along with dysfunction of pulmonary system [24], leading to epithelial cell damage and elevated vascular permeability. PM constitutes polyaromatic hydrocarbons (PAHs), predominantly benzo[a]anthracene, benzo[b] fluoranthene, benzo[k]fluoranthene, and benzo[a] pyrene, which possess carcinogenicity, as stated by the International Agency for Research on Cancer (IARC) [25]. The PAHs triggers the inflammation in epithelial cells and macrophages. This produces ROS to trigger lipid peroxidation [26]. ROS measurement is done by 2′,7′ dichlorofluorescin diacetate (DCFDA) assay on conclusion of the experiment. The ROS level in the control chip containing the healthy live monolayer of lung epithelial cells was significantly lower than the PM10-treated chips, while there is a relative elevation of ROS induction in the lung monolayer epithelial chips due to PM concentration. The control chip in Fig. 6a shows less fluorescence compared to Fig. 6b and c, and Fig. 6d indicates a decrease in fluorescence.

2.7 Mucin Release and Cytokine Analysis

Mucin is a major secretory glycoprotein with potential as a biomolecule to observe bronchioalveolar lavage and sputum samples of asthmatic patients. In the PM-treated chips, mucin levels increased. Mucin secretion in serum media was measured to be dependent on time and dose. Bronchoconstriction with decreased mucociliary clearance is a result of exposure to oxidative environment. Exposure of two days of high concentration PM, 400 pg/ml initiated mucin release, as shown in Fig. 7a.

IL-13 plays a critical role in the progression of asthma [27]. Moreover, it directly affects the epithelium layer of the human airways and is involved in causing respiratory tract inflammation, hyper-responsiveness of respiratory tract, hyperplasia of goblet cells, hypersecretion of mucus, and fibrosis of subepithelial layers, similar to that observed in the airway mucosa of individuals with asthma [28, 29]. Our experiment reports the high concentration of IL-13 in

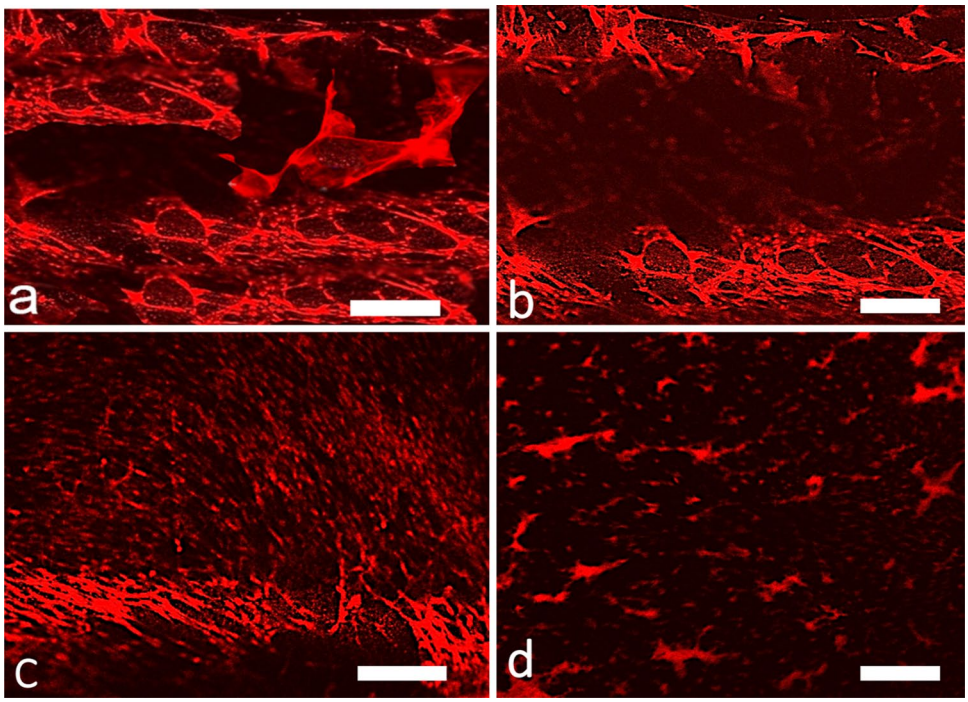

Fig. 4 Confocal micrographs of epithelial tight junctions in the control and PM10 in the treatment chips: **a** lung epithelial tight junctions stained with occludin conjugated Alexa Fluor 594 showing intracellular junctions; **b** PM-treated chip with concentration of 7.5 µg/ml showing some compromised integrity; **c** PM-treated chip with concentration of 37.5 µg/ml showing intracellular barrier damage; and **d** high concentration (151 µg/ml) of PM-treated chip showing diminishing expression of occluding. Scale bar: 100 µm

the media samples after 24-h exposure of PM10, and the extreme concentration was observed in samples with PM10 concentration of 151 µg/ml, as shown in Fig. 7c. Although the IL-13 levels remained high after 72 h, they showed a decreasing trend until ceasing after 96 h (Fig. 7c).

Cytokine interleukin-6 (IL-6) is also an inflammatory biomarker in spite of being originally an efficient modulator in triggering the immune responses [30]. The cytokine IL-6 is secreted from airway epithelium cells as an immune reaction as incidence of exposure to any allergen. Studies have recently determined that IL-6 plays an important role in the differentiation of effector $CD4^{+}$T cells as an adaptive immune response. Specifically, IL-6 suppresses Th1 and induces the differentiation of TH-2 to $CD4^{+}$T cells in separate regulatory cytokine pathways [28]. Numerous studies have documented the collective role of IL-6 and TGF-β for the promotion of murine Th-17 cells, whereas several others have suggested that IL-1β plays a more prominent role in promoting Th-17 [31, 32]. Our results indicated that lung epithelial cells release IL-6 in a damage-dependent manner, and high concentration of PM stimulus also results in much higher concentrations of IL-6 with time also in the media sample. The extreme concentration of the cytokine was detected after third day of the PM exposure, after which it tended to decrease (Fig. 7b). The pattern of cytokine discharge in the sample lung epithelial cells provided a very substantial information about the inflammation of the cells by PM10-induced stress in acute circumstances at 24 and 48 h after exposure (Fig. 7b). A well-studied biomarker and a cytokine TNF-α is secreted as an immune response of PM-induced stressed conditions in human beings, which is secreted by parenchymal cells of lungs after ROS production in mitochondria after damage to lung epithelial cells, leading to the activation of NF-kappa B signaling pathway. Figure 7 shows increased TNF-α concentrations at very high PM exposure levels. Conversely, the TNF-α levels at lower PM concentrations were comparatively low, and significant concentrations were only observed after 24 and 72 h of PM exposure (Fig. 7d) [33].

3 Discussion

This study reports establishment of a microphysiological system (MPS) for mechanical, environmental, chemical and toxicological analyses with efficient and robust abilities. Our unique microphysiological system comprises a sensor embedded chip with detachable glass-based and a transparent ITO-printed TEER electrode, an inhouse built microscope for online monitoring of different environmental conditions. Our MPS is unique in a way owing to its capacity to address previously reported limitations of this model.

The deadly respiratory illnesses such as asthma, COPD, and interstitial lung disease are mainly caused by PM environmental stress globally. The study of real-time environmental conditions is difficult in trans-well culture; therefore, drug development and efficient treatment for such harmful diseases leads to failure. Numerous studies have developed MPS for mimicking real-time phenomena; however, there have been several limitations, including lack of embedded

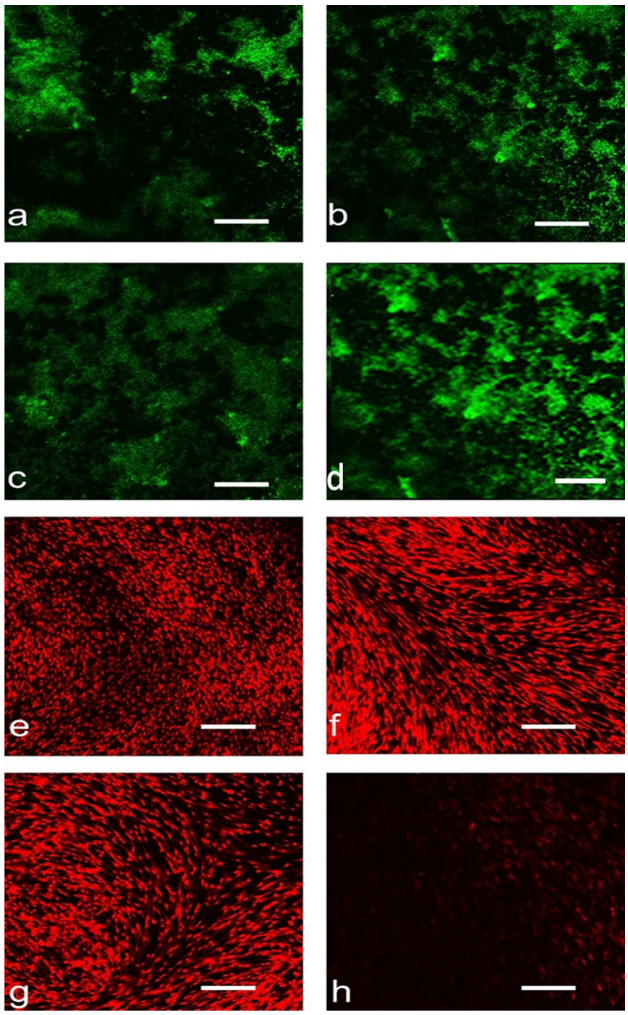

Fig. 5 Confocal micrograph of lung epithelial cells exhibiting goblet cell hyperplasia and decreased ciliated cell function in lung on chips after PM exposure; **a**–**d** lung on chip, human pulmonary epithelium stained with MUC5AC and attached with secondary Alexa Fluor goat anti mouse-488 control chip with media showing normal expression of mucin; **b** intensified mucin expression at PM concentration of 7.5 µg/ml; **c**, **d** high expression of mucin characteristic in asthmatic patients. Scale bar: 100 µm. **e**–**h** Diminishing expression of ciliated cell function with rising intensity of the PM10 exposure stained with primary Antiβ tubulin IV antibody followed by secondary Alexa flour, goat anti-rabbit 555 (H + L) red showing loss of movement of the AT type-II ciliated cell function

sensors and PDMS-based chips [34]. In the current study, we introduced a model with primary lung distal airway monolayer on a glass chip, which provided the characterization of our MPS, system integrated sensors, and real-time microscope. We attempted to mimic the disease conditions associated with PM exposure, which was characterized by the biomarker detection of the secretory cytokine IL-6, TNF-α, IL-13, and mucin immunofluorescence analysis. Tight junctions and barrier integrity of the healthy monolayer of distal airways on chips were determined by occludin expression. This milestone was accomplished by selecting three different levels of PM set by daily climate control conditions of the country: good, fair, and bad, by following the exposure scheme of PM an individual can experience in working days. Earliest, we tried to validate the permeability of the lung airway monolayer with the help of immunofluorescence analysis by confocal microscopy and TEER. Then, we initiated exposure of the PM to produce PM stressed environment in our microfluidic cell culture system with three distinctive concentrations for four days and daily exposures of eight hours. For toxicity evaluation, samples from circulating media were collected 12 h after the first exposure and then after every 24 h, and impedance was determined every 30 min to characterize changes in the permeability of the epithelium. A software was installed in the computer to automatically record the results of the TEER and real-time microscope attached with our MPS.

Barrier junctions integrity was increased up to 80% for the first four days in all the experimental and control chips; according to the data from the TEER software, it is also demonstrated that PM-exposed chips showed compromised permeability of the barrier after 12 h of exposure, and increasing toxicity leads to increased concentration of inflammatory signaling molecules evaluated later with the help of ELISA.

The conditions of diseased and normal treated were analyzed by immunofluorescence assay. Significant differences were observed in occludin expression. This impacted the barrier junctions of control and PM-treated chips. PM-treated chips reveled boosted inflammation. Moreover, mucin and anti-β tubulin IV biomarkers specifically used for morphology analysis provided a complete overview of the experimental results. Asthmatic patients have mucin-enriched lung epithelium cells. The ciliated cells function along with movement of mucociliary cells that stops due to pulmonary stress. Pulmonary stress further aggravates hyper-responsiveness. Mucin production is promoted by IL-13 by higher recruitment of eosinophil in the system. Cytokine inductions and release are promoted by exposure to PM in 24 h along with IL-13.

Mucin release is associated with IL-13, and proliferation in the absorption of mucin released from lung epithelial cells is evidence of the malfunctioning of ciliated cells that are convoluted in clearance of mucociliary. The graph of mucin ELISA complemented the fluorescent microscopic images and validated our MPS's ability to recapitulate physiology of human at the alveolar level by displaying increasing concentrations of mucin at high concentrations of PM and long-lasting exposure. Such biomarkers could be used to indicate increased incidences of numerous disorders in our sophisticated and automated MPS model. Interleukin-6 is an inflammatory cytokine formed in COPD and asthma and is associated with acute compromised lung function [35]. In our study, the interleukin-6

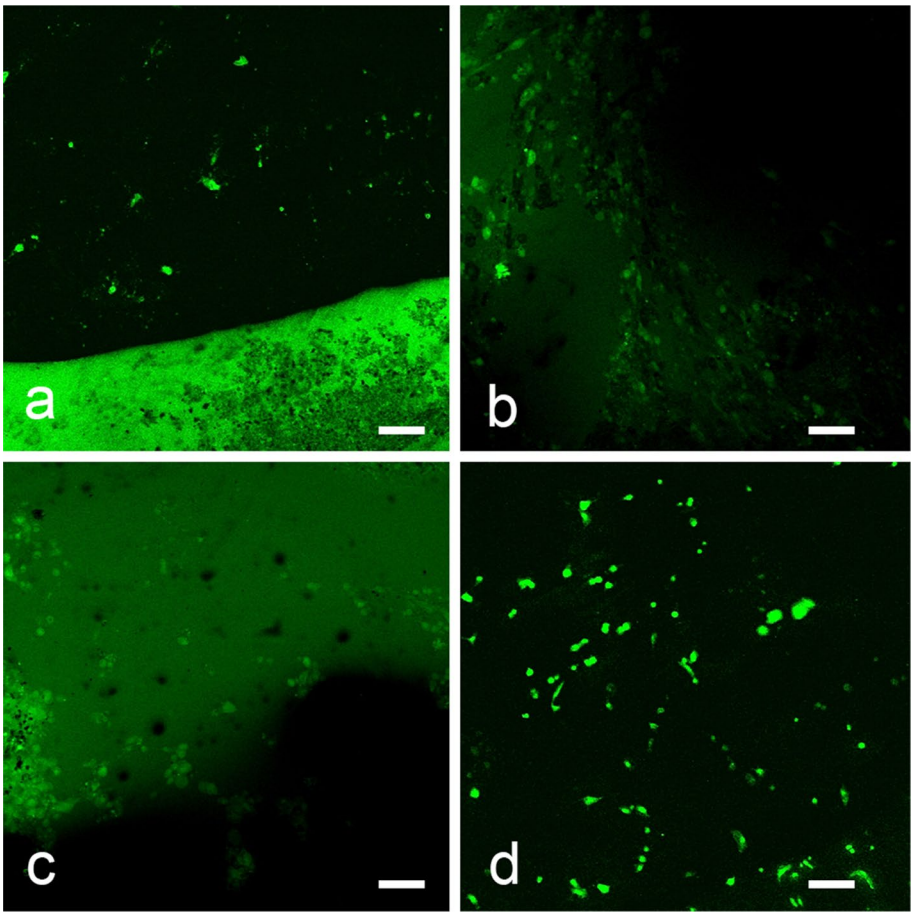

Fig. 6 Confocal micrographs of DCFDA assay for ROS detection: **a** normal positive control without PM exposure; **b** lung epithelial cells exposed to a PM concentration of 7.5 µg/ml showing ROS; **c**, **d** chips treated with PM concentrations of 37.5 µg/ml and 151 µg/ml showing increased ROS generation in the cellular environment. Scale bar: 100 µm

absorption presented a continuing proliferation in the production of these cytokines, which is typically observed in the sputum samples of asthma patients [36, 37]. Production of free radical and oxidative stress occur as inflaming responses associated with exposure of PM, as described previously in numerous studies [38–40]. Several studies have reported information of our MPS validity for fruitful analysis of toxicological and the reconstruction of pathophysiology of organ, and the future scope of our research is to study physiology of complex tissue with the incorporation of embedded sensors. The graph demonstrating levels of mucin in Fig. 7a, which shows a proliferation in the mucin released in the serum, is also similar with the confocal micrographs. In the future, this device will aid to design complex tissue of human physiology and disease models for toxicity testing. Moreover, organ-on-chip technology has provided suitable drug candidates during the COVID-19 pandemic.

4 Conclusion

Advancements in the technology of organ-on-chip offer efficient and robust solutions for discovery of drug and evaluation of therapeutics. Our MPS device has the potential to recapitulate the healthy and stressed human physiology. Findings of our study made us eligible to validate this well-equipped system, consisting of a reconfigurable microfluidic chip, a handheld real-time microscope live monitoring of the cells, and a system embedded TEER sensor, which are essential for mimicking the physiologically healthy and stressed MPS models of the human body. Metabolically active lung epithelial monolayer growth in optimized fluidic conditions was compared to less active monolayer in trans-well cultures. High cytokine levels were observed in all types of the disease models in this device due to optimized circulation of the fluid shear stress conditions. The main challenge in manufacturing an MPS is to replicate the in vivo like conditions for accommodating an organ reliably and robustness. First, the difficulty associated with reconstructing the in vivo environment for housing an organ. The second challenge of MPS's production is the development of a low-cost toxicity score using a sensor embedded in the system. In this study, these challenges partially fulfilled the need for a robust and effective Microphysiological system (MPS). This device provides preliminary data for a breakthrough in MPS development technology. In upcoming researches, our research will aim to construct complex tissue mimics of the human lung organ for toxicity analysis and discovery of novel drugs by

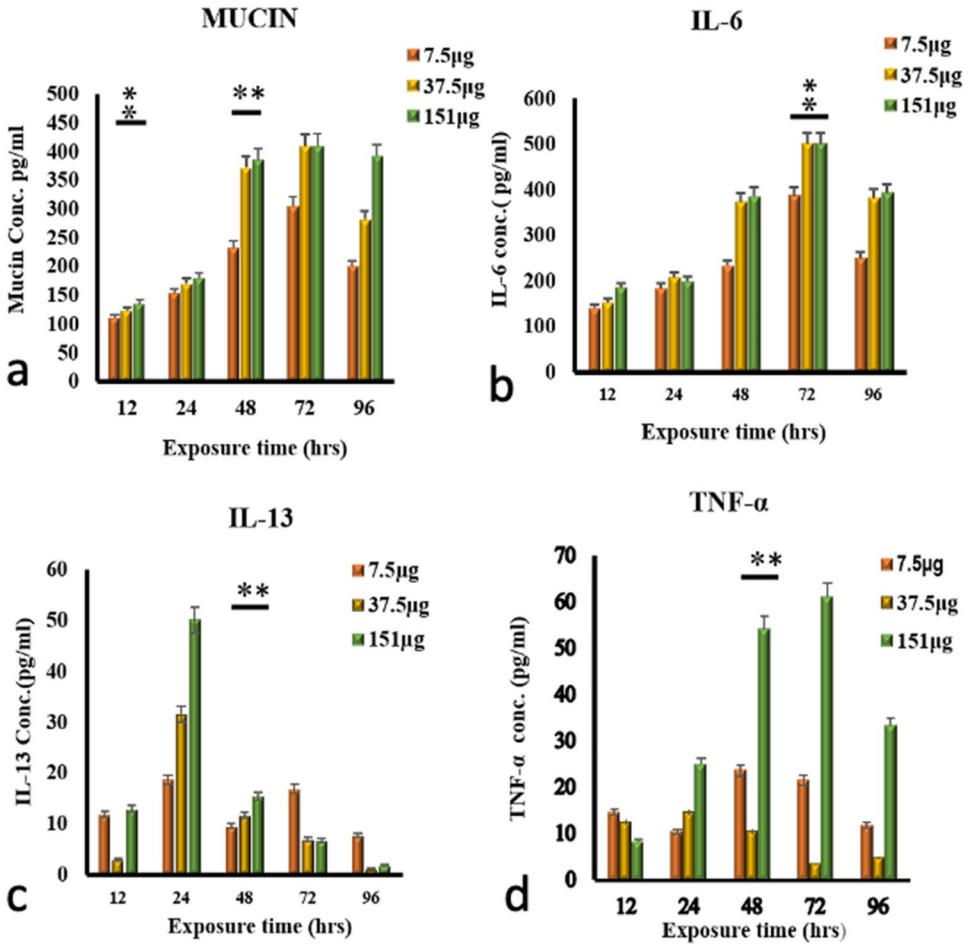

Fig. 7 Cytokine concentration (pg/ml) vs. exposure time. **a** MUC5AC discharge in the serum of the microfluidic environment was analyzed as dose and time-dependent because highly oxidative stress conditions lead to high Mucin production and less ciliary movements. By the end of the of particulate matter (PM10) exposure, high concentration of PM10 leads to the discharge of 400 pg/ml mucin. The '*' denotes significant results ($p < 0.05$), and '**' denotes highly significant results ($p < 0.001$); **b** IL-6 concentration in cell culture media recorded at 12, 24, 48,72, and 96 h. The concentration increased after 24 h and, as for ROS production, recorded a high concentration at 96 h until the end of the experiment; **c** **IL-13 secretion in serum was analyzed after 12 h of PM10 exposure. The highest concentration was recorded at 24 h and decreased with time until 96 h; **d** TNF-α concentration showed dose-dependent pattern of cytokine release with respect to PM exposure. The lowest TNF-α concentration recorded in the cell culture media was approximately 30 pg/ml, and at high PM-concentration exposures, release of cytokine was maximum after 3 d of exposure

using system incorporated pathological sensors to substitute the molecular investigation of pathological disorders. Furthermore, we would like to apply these similar 3D MPS concept to other tissue organ, such as liver.

5 Materials and Methods

5.1 Chemical and Materials

Particulate matter PM10 organic components reference material ERM(CZ-100) and inorganic components ERM CZ-120 were bought from JRC Joint research commission Europe and characterized by SEM Analysis (Scanning Electron microscopy (MIRA-3 TESCAN). Three different concentrations (good, fair, and bad) of the PM10 were manufactured according to daily update of climate control department, South Korea. Stock solution of equimolar components of the PM10 was prepared under sterile environmental conditions in the BSL-2 laboratory facility. Equimolar components of PM10 were resuspended in the Alveolar epithelial growth medium and followed by 60-min sonication for deagglomeration.

5.2 Chip Design and Sensor Development

The chip (BioSpero) was constructed using top and bottom glass ($W = 56$ mm, $H = 41$ mm, $T = 1.1$ mm). Based on the

3D printing technology, a microchannel and cell culture chamber were implemented using a silicon elastomer material (Musil Medical Grade Silicone MED-6033). For cell culture, the channel is printed in 15 mm size on the bottom glass, and the channel and the cell culture chamber are connected. The TEER sensor was coated with indium tin oxide (ITO) to achieve an electrode of length 4 mm and thickness 500 nm. The ITO electrodes coated on the upper and lower glasses were fixed at the same position using a chip holder (BioSpero), and a circuit was implemented to measure electrical impedance. One Indium Tin Oxide printed TEER electrode was 4 mm^2. Electrical resistance was measured in Ohms (Ω mm^2). LabVIEW software monitoring was activated by connecting a connector to the ITO electrode, and resistance values that could check the cell state were measured. (Supplementary Fig. 1).

An A120 portable microscope was developed to monitor the state of cells in real time using a TEER sensor. The microscope consisted of a Plain Achromatic Objective 121 (AmScope TM) and an SCMOS series 122 USB 2.0 eyepiece camera (ToupTek TM) assembled using a 3D printer. A blue wavelength 469 ± 17.5 nm filter was used. Moreover, camera control software (ToupTek TM) was used for high-speed visualization of the images and video processing. Calibrations of real-time microscopes and TEER sensors are described in our previous papers [9, 41]. In order to simulate the dynamic environment of the human body, the peristaltic pump was connected to a chip and the culture solution was circulated. The flow rate of the culture solution was corrected to simulate the human lung cell shear stress, and the shear stress was 8 dyne/cm^2 [42]. The culture solution velocity was fixed at 80 µl/ml to maintain 8 dyne/cm^2 shear stress in the lung epithelial cell monolayer. The microchannel of the designed chip experiencing shear stress induced by cell culture medium on the cells was calculated using the following equation [43].

$$\tau = 6\mu Q/(wh^2)$$

where μ denotes the viscosity of the media, Q denotes the media flow rate, w denotes the width, and h denotes the height of the microfluidic channel.

5.3 Microfluidic Cell Culture Maintenance

Human small airway epithelial cells and human pulmonary alveolar type-I and type-II cells were purchased from Lonza and ScienCell, respectively, and then revived by following the company's protocol. T-25 flask (Corning) at a concentration of 2 µg/cm^3 was coated with Poly-L lysine (Sigma-Aldrich) and incubated at 37 °C overnight. The flask was washed mildly before adding a cell culture medium comprising an alveolar epithelial cell medium (AEpiCM, Cat. #3201), MEM, epithelial growth supplement (5 ml), 10% FBS, a 1% penicillin streptomycin solution, and 5% carbon dioxide at 37 °C. Before seeding, chip bottom glasses were sterilized for 1 h in UV and coated overnight with 10 µg of a 0.01% ECM collagen solution type-I (Sigma Cat # C3867) suspended in DPBS before seeding the cells. Upon reaching a $< 90\%$ confluence at passage 2, human pulmonary alveolar type-I and type-II cells and small airway epithelial cells at a density of 2.27×10^5 were seeded onto the chip with a TEER electrode. Cells were seeded on ECM-coated chips for 4 h, and the culture medium was circulated at a flow rate of 120 µl/min using a peristaltic pump. Moreover, TEER sensors and microscopes were placed for real-time monitoring of cell state. After 12 h, the flow rate of the cell culture medium was set at 60 µl/min; after 48 h, fresh media was supplied to the media reservoir. The chip was later introduced to three different concentrations of particulate matter to access the toxicity in human lung distal airways model.

5.4 Membrane Barrier Integrity Determination

The lung epithelial cell tight junctions were confirmed by the resistance value measured by the TEER sensor. Lung epithelial cells were stained for immunofluorescence analysis by staining for the tight junction epithelial cell marker occludin conjugated with Alexa Fluor 594 (Sigma (OC-3F10). For staining, the cells were PBS-washed 5 times, 4% paraformaldehyde helped to fix the cells 15 min, permeated with 0.2% Triton X-100 (Sigma) for 20 min, blocked with 5% BSA suspended in PBS at room temperature for 60 min, and incubated with occludin-conjugated Alexa Fluor 594 (1:200) for 4 h. After incubating, the samples were observed under a fluorescent microscope [8].

5.5 Fluorescent Microscopy of Mucociliary Clearance

For immunocytochemical analysis, lung epithelial mucus-secreting goblet and ciliated cells were stained. The lung epithelial cell chip was washed using PBS, and fixation was done with 4% paraformaldehyde and then for more 15 min washed with PBST three times. The cells on the chips were permeabilized in the presence of 0.1% triton 100-X by incubating for 20 min at room temperature and blocked with 1%BSA for half an hour at room temperature proceeded by attaching monoclonal antibody 1:1000 MUC5AC (45M1), (1:500) anti-β tubulin IV (ab11315) Abcam antibodies, goat anti-mouse (H + L), 488 green (A28175), and goat anti-rabbit 555 (H + L) red (A-21428), secondary Alexa Flours correspondingly, and images were taken for proper morphological analysis, under a fluorescent microscope (Zeiss Germany).

5.6 ROS Measurement/DCFDA Analysis

Cell death and functional loss lead to the defense mechanisms activation which discharge intracellular ROS and antioxidant species, anti-inflammatory and pro-inflammatory biomolecules, stimulate genotoxicity [44–46]. ROS generation is responsible for mitochondrial damage and increasing the acidity of the cellular environment, leading to high rates of chronic inflammation. Moreover, continuous exposure to pollutants and xenobiotic in air are the main cause of numerous respiratory illnesses, including asthma and COPD. For ROS analysis after PM10 exposure, the three different concentrations of PM were evaluated for four days long exposure with the normal healthy controls' chips. The cells on the chips were PBS-washed, and they were allowed to incubate incubator at 37 °C in 5% CO_2 with the dye (CM-H2DCFDA) 50 µM (Sigma D6883) probed in PBS and incubated for 30 min. After completing incubation, the cells of the chips were washed with PBS solution and again incubated for more 5 min with 90% dimethyl sulfoxide (DMSO) (Sigma D2438) in PBS. The cells' containing chip was washed and visualized by a fluorescent microscope.

5.7 Cytokines Analysis and Oxidative Stress Under PM10 Exposure

The real-time PM exposure model on a chip recapitulating an in vivo diseased condition was developed in this study, and complete cytokine signaling information was used for the characterization. As inflammation starts upon the airway cells, neutrophil uptake also increases; here, the cytokines produced (IL-6, IL-13, TNF-α, mucin, and reactive oxygen species) as incidence of asthma and allergic disease are possible mediators of the of asthma attack due to long-term PM exposure of the lung airways. Moreover, the release of IL-13 from inflamed cells of the distal airway provides data on the prevalence of COPD, TNF-α, oxidative stress, and ROS production, which result in cell death in airway cells. Mucus hypersecretion and metaplasia of mucin-producing cells in the human distal airways are termed pathological states which usually arise on the commencement of severe respiratory conditions, such conditions activated with $CD4^+$ Th2-type immune response in the human lung. This $CD4^+$ Th2-type immune response can be evaluated by IL-13 secretion in the lung microenvironment, along with little secretion of Th1 cytokines for example IFNγ [47]. The cytokine environment and physical foundations of the lungs determine and the fate of effector $CD4^+$ T cells, which is one of the very crucial factors in triggering local immune response. Parenchymal cells of the lungs are not considered as the part of immune system, but they also help to trigger a type of an immune response by secretion of certain biomolecules. Lung parenchymal cells secrete one of the key cytokine IL-6 which is involved in various inflammatory pathways [48, 49]. IL -6 is produced by lung epithelial cells, and relatively increased secretions of IL-6 have been detected in asthmatic patients [50]. Under the PM exposure responses, (TNF-α) and IL-6 are secreted as the vital intermediaries of the inflammatory biomarkers of the lung airways, several human sample-based studies in vitro, and in vivo.

The present study selected biomarkers for asthma and COPD, i.e., TNF-α, interlukin-13, interlukin-6, and mucin. Cytokines were measured from all the control and experimental media reservoirs after first 24 h of the experiment. Cytokine analysis measurement on the selected biomarkers, i.e., IL-13, IL-6 and TNF-α, was performed using enzyme-linked immunosorbent assay (ELISA) kits by the standard protocol and instructions of the manufacturing company. MUCIN ELISA kit was also used for mucin analysis and was performed by the sandwich method [51].

5.8 Statistical Representation of Experimental Data

Data were presented as the mean ± standard error of the mean (SEM). Statistical analysis was performed on the experimental data by comparing controls with experimental data sets using Tukey's multiple comparison tests and ANOVA with full-factorial analysis. Microsoft Excel was used for all the statistical analyses. The value $p < 0.05$ was showing significant (*), and the value $p < 0.01$ was showing highly significant (**). Experimental data were collected in triplicates.

Supplementary Information The online version contains supplementary material available at https://doi.org/10.1007/s13206-022-00068-x.

Acknowledgements This research was supported by the Technology Innovation Program (or Industrial Strategic Technology Development Program-Development of disease models based on 3D microenvironmental platform mimicking multiple organs and evaluation of drug efficacy) (20008413) funded By the Ministry of Trade, Industry & Energy (MOTIE, Korea).

Author contributions FJ did whole experiments in this manuscript. FJ and YSK designed experiments scheme. FJ and SHL wrote the manuscript, and then SHL revised the manuscript. All authors read and approved the final manuscript.

Declarations

Conflict of interest The authors declare that they have no competing interests.

References

1. Lelieveld, J., Evans, J.S., Fnais, M., Giannadaki, D., Pozzer, A.: The contribution of outdoor air pollution sources to premature mortality on a global scale. Nature **525**, 367–371 (2015)

2. Gilmour, M.I., Daniels, M., McCrillis, R.C., Winsett, D., Selgrade, M.K.: Air pollutant-enhanced respiratory disease in experimental animals. Environ. Health Perspect. **109**, 619–622 (2001)
3. Becker, S., Mundandhara, S., Devlin, R.B., Madden, M.: Regulation of cytokine production in human alveolar macrophages and airway epithelial cells in response to ambient air pollution particles: further mechanistic studies. Toxicol. Appl. Pharmacol. **207**, 269–275 (2005)
4. Brook, R.D., et al.: Particulate matter air pollution and cardiovascular disease: an update to the scientific statement from the American Heart Association. Circulation **121**, 2331–2378 (2010)
5. Woods, A., Brull, D., Humphries, S., Montgomery, H.: Genetics of inflammation and risk of coronary artery disease: the central role of interleukin-6. Eur. Heart J. **21**, 1574–1583 (2000)
6. Ingram, J.L., Kraft, M.: IL-13 in asthma and allergic disease: asthma phenotypes and targeted therapies. J. Allergy Clin. Immunol. **130**, 829–842 (2012)
7. Martignoni, M., Groothuis, G.M., de Kanter, R.: Species differences between mouse, rat, dog, monkey and human CYP-mediated drug metabolism, inhibition and induction. Expert Opin. Drug Metab. Toxicol. **2**, 875–894 (2006)
8. Huh, D., Matthews, B.D., Mammoto, A., Montoya-Zavala, M., Hsin, H.Y., Ingber, D.E.: Reconstituting organ-level lung functions on a chip. Science **328**, 1662–1668 (2010)
9. Asif, A., Kim, K.H., Jabbar, F., Kim, S., Choi, K.H.: Real-time sensors for live monitoring of disease and drug analysis in microfluidic model of proximal tubule. Microfluid. Nanofluid. **24**, 1–10 (2020)
10. Zhang, Y.S., Aleman, J., Shin, S.R., Kilic, T., Kim, D., Shaegh, S.A.M., Massa, S., Riahi, R., Chae, S., Hu, N.: Multisensor-integrated organs-on-chips platform for automated and continual in situ monitoring of organoid behaviors. Proc. Natl. Acad. Sci. **114**, E2293–E2302 (2017)
11. Thuenauer, R., Rodriguez-Boulan, E., Römer, W.: Microfluidic approaches for epithelial cell layer culture and characterisation. Analyst **139**, 3206–3218 (2014)
12. Booth, R., Kim, H.: Characterization of a microfluidic in vitro model of the blood-brain barrier (μBBB). Lab Chip **12**, 1784–1792 (2012)
13. Booth, R., Noh, S., Kim, H.: A multiple-channel, multiple-assay platform for characterization of full-range shear stress effects on vascular endothelial cells. Lab Chip **14**, 1880–1890 (2014)
14. Yeste, J., Illa, X., Gutiérrez, C., Solé, M., Guimerà, A., Villa, R.: Geometric correction factor for transepithelial electrical resistance measurements in transwell and microfluidic cell cultures. J. Phys. D: Appl. Phys. **49**, 375401 (2016)
15. Odijk, M., et al.: Measuring direct current trans-epithelial electrical resistance in organ-on-a-chip microsystems. Lab Chip **15**, 745–752 (2015)
16. Srinivasan, B., et al.: TEER measurement techniques for in vitro barrier model systems. J. Lab. Autom. **20**, 107–126 (2015)
17. Chen, X., Feng, Q., Zhang, Y., Zhang, Y.: Insights into a deterministic lateral displacement sorting chip with new cross-section micropillars. Chaos Solitons Fractals **156**, 111884 (2022)
18. Soomro, A.M., et al.: All-range flexible and biocompatible humidity sensor based on poly lactic glycolic acid (PLGA) and its application in human breathing for wearable health monitoring. J. Mater. Sci. Electron. **30**, 9455–9465 (2019)
19. Kirkham, S., Sheehan, J.K., Knight, D., Richardson, P.S., Thornton, D.J.: Heterogeneity of airways mucus: variations in the amounts and glycoforms of the major oligomeric mucins MUC5AC and MUC5B. Biochem. J. **361**, 537–546 (2002)
20. Morcillo, E.J., Cortijo, J.: Mucus and MUC in asthma. Curr. Opin. Pulm. Med. **12**, 1–6 (2006)
21. Prahalad, S., Bove, K.E., Dickens, D., Lovell, D.J., Grom, A.A.: Etanercept in the treatment of macrophage activation syndrome. J. Rheumatol. **28**, 2120–2124 (2001)
22. Billet, S.: The theologies of transparency in Europe: the limits and possibilities of 'fusion'in the EU transparency regime. J. Public Aff. **7**, 319–330 (2007)
23. Stohs, S.J., Bagchi, D.: Oxidative mechanisms in the toxicity of metal ions. Free Radic. Biol. Med. **18**, 321–336 (1995)
24. Chauhan, S.S., Misra, U.K.: Elevation of rat pulmonary, hepatic and lung surfactant lipids by fly ash inhalation. Biochem. Pharmacol. **41**, 191–198 (1991)
25. Castano-Vinyals, G., D'errico, A., Malats, N., Kogevinas, M.: Biomarkers of exposure to polycyclic aromatic hydrocarbons from environmental air pollution. Occup. Environ. Med. **61**, e12–e12 (2004)
26. Thomsen, A.E., et al.: Prodrugs of purine and pyrimidine analogues for the intestinal di/tri-peptide transporter PepT1: affinity for hPepT1 in Caco-2 cells, drug release in aqueous media and in vitro metabolism. J. Control. Release. **86**, 279–292 (2003)
27. Kelly-Welch, A., Hanson, E.M., Keegan, A.D.: Interleukin-13 (IL-13) pathway. Sci. STKE **2005**, cm8–cm8 (2005)
28. Dienz, O., Rincon, M.: The effects of IL-6 on CD4 T cell responses. Clin. Immunol. **130**, 27–33 (2009)
29. Kuperman, D.A., et al.: Direct effects of interleukin-13 on epithelial cells cause airway hyperreactivity and mucus overproduction in asthma. Nat. Med. **8**, 885–889 (2002)
30. Kamimura, D., Ishihara, K., Hirano, T.: IL-6 signal transduction and its physiological roles: the signal orchestration model. Rev. Physiol. Biochem. Pharmacol. (2003). https://doi.org/10.1007/s10254-003-0012-2
31. Acosta-Rodriguez, E.V., Napolitani, G., Lanzavecchia, A., Sallusto, F.: Interleukins 1β and 6 but not transforming growth factor-β are essential for the differentiation of interleukin 17–producing human T helper cells. Nat. Immunol. **8**, 942–949 (2007)
32. Bettelli, E., et al.: Reciprocal developmental pathways for the generation of pathogenic effector TH 17 and regulatory T cells. Nature **441**, 235–238 (2006)
33. Lakshmanan, I., et al.: Mucins in lung cancer: diagnostic, prognostic, and therapeutic implications. J. Thorac. Oncol. **10**, 19–27 (2015)
34. Barnes, P.J.: The cytokine network in asthma and chronic obstructive pulmonary disease. J. Clin. Investig. **118**, 3546–3556 (2008)
35. Grubek-Jaworska, H., et al.: IL-6 and IL-13 in induced sputum of COPD and asthma patients: correlation with respiratory tests. Respiration **84**, 101–107 (2012)
36. Yang, B., Chen, D., Zhao, H., Xiao, C.: The effects for PM2. 5 exposure on non-small-cell lung cancer induced motility and proliferation. Springerplus **5**, 1–9 (2016)
37. González-Flecha, B.: Oxidant mechanisms in response to ambient air particles. Mol. Aspects Med. **25**, 169–182 (2004)
38. Nam, K.H., Li, J.: BRI1/BAK1, a receptor kinase pair mediating brassinosteroid signaling. Cell **110**, 203–212 (2002)
39. Ootsubo, T., Usui, F., Kawakita, H., Ishiguro, M., Furusho, R., Hasegawa, S., Ueno, M., Watanabe, J.-I., Sekiguchi, T., Wada, T.: Detection of parent H2O and CO2 molecules in the 2.5–5 μm spectrum of comet C/2007 N3 (Lulin) observed with AKARI. Astrophys. J. Lett. **717**, L66 (2010)
40. Khalid, M.A.U., et al.: A lung cancer-on-chip platform with integrated biosensors for physiological monitoring and toxicity assessment. Biochem. Eng. J. **155**, 107469 (2020)
41. Essig, M., Friedlander, G.: Tubular shear stress and phenotype of renal proximal tubular cells. J. Am. Soc. Nephrol. **14**, S33–S35 (2003)
42. Vormann, M.K., et al.: Nephrotoxicity and kidney transport assessment on 3D perfused proximal tubules. AAPS J. **20**, 1–11 (2018)

43. Bakand, S., Hayes, A., Dechsakulthorn, F.: Nanoparticles: a review of particle toxicology following inhalation exposure. Inhal. Toxicol. **24**, 125–135 (2012)
44. Johnston, H., et al.: Engineered nanomaterial risk. Lessons learnt from completed nanotoxicology studies: potential solutions to current and future challenges. Crit. Rev. Toxicol. **43**, 1–20 (2013)
45. Stone, V., Johnston, H., Schins, R.P.: Development of in vitro systems for nanotoxicology: methodological considerations. Crit. Rev. Toxicol. **39**, 613–626 (2009)
46. Georas, S., Guo, J., De Fanis, U., Casolaro, V.: T-helper cell type-2 regulation in allergic disease. Eur. Respir. J. **26**, 1119–1137 (2005)
47. Cromwell, O., et al.: Expression and generation of interleukin-8, IL-6 and granulocyte-macrophage colony-stimulating factor by bronchial epithelial cells and enhancement by IL-1 beta and tumour necrosis factor-alpha. Immunology **77**, 330 (1992)
48. King, C., Brennan, S., Thompson, P.J., Stewart, G.A.: Dust mite proteolytic allergens induce cytokine release from cultured airway epithelium. J. Immunol. **161**, 3645–3651 (1998)
49. Kicic, A., Sutanto, E.N., Stevens, P.T., Knight, D.A., Stick, S.M.: Intrinsic biochemical and functional differences in bronchial epithelial cells of children with asthma. Am. J. Respir. **174**, 1110–1118 (2006)
50. Marini, M., Vittori, E., Hollemborg, J., Mattoli, S.: Expression of the potent inflammatory cytokines, granulocyte-macrophage-colony-stimulating factor and interleukin-6 and interleukin-8, in bronchial epithelial cells of patients with asthma. J. Allergy Clin. Immunol. **89**, 1001–1009 (1992)
51. Lee, H.J., et al.: Suppressive effects of coixol, glyceryl trilinoleate and natural products derived from Coix Lachryma-Jobi var. ma-yuen on gene expression, production and secretion of airway MUC5AC mucin. Arch. Pharm. Res. **38**, 620–627 (2015)